BIOCHEMISTRY
including biophysical chemistry & molecular biology

Article

pubs.acs.org/biochemistry

Active Site and Remote Contributions to Catalysis in Methylthioadenosine Nucleosidases

Keisha Thomas,[†] Scott A. Cameron,[†] Steven C. Almo,[†] Emmanuel S. Burgos,[†] Shivali A. Gulab,[‡] and Vern L. Schramm*,[†]

[†]Department of Biochemistry, Albert Einstein College of Medicine, 1300 Morris Park Avenue, Bronx, New York 10461, United States
[‡]The Ferrier Research Institute, Victoria University of Wellington, Wellington, New Zealand

Supporting Information

ABSTRACT: 5′-Methylthioadenosine/*S*-adenosyl-L-homocysteine nucleosidases (MTANs) catalyze the hydrolysis of 5′-methylthioadenosine to adenine and 5-methylthioribose. The amino acid sequences of the MTANs from *Vibrio cholerae* (*Vc*MTAN) and *Escherichia coli* (*Ec*MTAN) are 60% identical and 75% similar. Protein structure folds and kinetic properties are similar. However, binding of transition-state analogues is dominated by favorable entropy in *Vc*MTAN and by enthalpy in *Ec*MTAN. Catalytic sites of *Vc*MTAN and *Ec*MTAN in contact with reactants differ by two residues; Ala113 and Val153 in *Vc*MTAN are Pro113 and Ile152, respectively, in *Ec*MTAN. We mutated the *Vc*MTAN catalytic site residues to match those of *Ec*MTAN in anticipation of altering its properties toward *Ec*MTAN. Inhibition of *Vc*MTAN by transition-state analogues required filling both active sites of the homodimer. However, in the Val153Ile mutant or double mutants, transition-state analogue binding at one site caused complete inhibition. Therefore, a single amino acid, Val153, alters the catalytic site cooperativity in *Vc*MTAN. The transition-state analogue affinity and thermodynamics in mutant *Vc*MTAN became even more unlike those of *Ec*MTAN, the opposite of expectations from catalytic site similarity; thus, catalytic site contacts in *Vc*MTAN are unable to recapitulate the properties of *Ec*MTAN. X-ray crystal structures of *Ec*MTAN, *Vc*MTAN, and a multiple-site mutant of *Vc*MTAN most closely resembling *Ec*MTAN in catalytic site contacts show no major protein conformational differences. The overall protein architectures of these closely related proteins are implicated in contributing to the catalytic site differences.

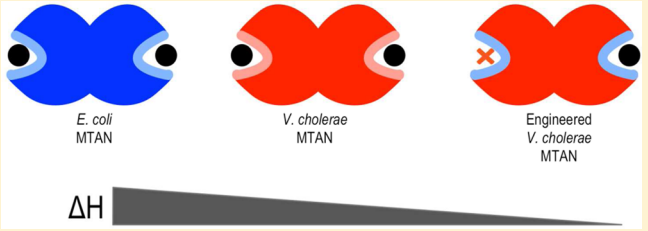

5′-Methylthioadenosine/*S*-adenosyl-L-homocysteine nucleosidase (MTAN, EC 3.2.2.16) from *Vibrio cholerae* catalyzes the hydrolysis of 5′-methylthioadenosine (MTA) to adenine and 5-methylthioribose (MTR).[1] MTANs are involved in the pathways of autoinducer-1 and autoinducer-2 quorum sensing in Gram-negative bacteria. Thus, inhibition of MTANs interferes with pathogenicity functions associated with quorum sensing.[2] In a few microorganisms, including *Helicobacter pylori*, MTAN is also required for menaquinone synthesis, an essential pathway for electron transport. In these organisms, MTAN inhibition provides a unique antibiotic approach by targeting menaquinone synthesis.[3−5]

The amino acid sequence of *Vc*MTAN is 60% identical and 75% similar to that of *Ec*MTAN (Figure S1 of the Supporting Information). Both MTANs are homodimers with similar protein folds and a single active site per monomer. The energetics of binding of picomolar affinity transition-state analogues to *V. cholerae* MTAN (*Vc*MTAN) indicate that favorable entropic contributions dominate binding, with smaller favorable enthalpic contributions.[6] In contrast, binding of the inhibitor to *Escherichia coli* MTAN (*Ec*MTAN) is dominated by a large favorable enthalpy accompanied by smaller but also favorable entropic factors.[6]

Analysis of the amino acid sequence and X-ray crystal structures of *Vc*MTAN and *Ec*MTAN in complex with 4′-deaza-1′-aza-2′-deoxy-1′-(9-methylene)-Immucillin-A (DADMe-ImmA) and similar compounds revealed only two differences in the amino acid residues directly in contact with the bound inhibitor (Figure 1 and Figure S1 of the Supporting Information). At position 113, there is an alanine in *Vc*MTAN and a proline in *Ec*MTAN. The residue at position 113 is located on a loop structure that interacts with the 5′-region of the bound substrate or inhibitor at the active site of the adjacent monomer. Ala113 contributes a hydrophobic interaction to the 5′-group of the inhibitor near the solvent interface of the active site.[7]

In *Ec*MTAN, residue 152 is an isoleucine, while its analogous residue in *Vc*MTAN is Val153. The main chain nitrogen and oxygen of Val153 in *Vc*MTAN form hydrogen bonds to N1 (H-bond length of 3.1 Å) and N6 (H-bond length of 2.9 Å), respectively, of the deazaadenine base of BuTDIA (Figure S3 of the Supporting Information). If either of these hydrogen bonds

Received: December 4, 2014
Revised: March 23, 2015
Published: March 25, 2015

DOI: 10.1021/bi501487w
Biochemistry 2015, 54, 2520−2529

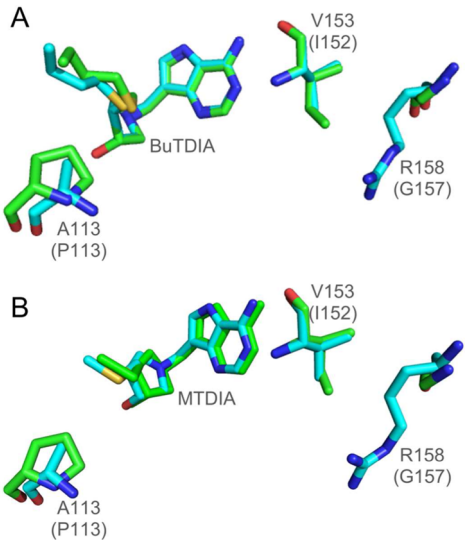

Figure 1. Structures of select residues of *Ec*MTAN (green) and *Vc*MTAN (blue) in the active sites bound to transition-state analogues. The top label corresponds to the residue numbering and identity in *Vc*MTAN, while the bottom label (in parentheses) corresponds to analogous residues in *Ec*MTAN. (A) Structural orientation of selected active site residues in complex with BuTDIA in the active sites of *Vc*MTAN and *Ec*MTAN. (B) Structural orientation of selected active site residues in complex with MTDIA in the active sites of *Vc*MTAN and *Ec*MTAN.

is weakened in $VcMTAN_{V153I}$, one would expect a decrease in binding energy for BuTDIA.

In silico mutations of Ile153 and Ala113 in *Vc*MTAN to the analogous residues found in *Ec*MTAN (Val152 and Pro113, respectively) are predicted to be compatible with the overall structure, with the preservation of similar hydrogen bonding distances to the bound inhibitor (Figure S4 of the Supporting Information). However, the *in silico* single mutant, Val153Ile, of *Vc*MTAN predicted that one of the isoleucine rotamers had the potential for steric hindrance with the neighboring Arg158 located at the dimer interface (Figure 1 and Figure S4 of the Supporting Information). Significantly, the residue corresponding to Arg158 in *Ec*MTAN is glycine. On the basis of these differences, we also investigated the effect of the triple mutant, $VcMTAN_{A113P/V153I/R158G}$ ($VcMTAN_{TRIPLE}$), all of which mutate the *Vc*MTAN structure toward *Ec*MTAN. Analyses of 17 individual active site mutations in *Ec*MTAN have been performed in prior studies, yet the effects of mutations at positions 113, 153, and 158 (*Vc*MTAN numbering) have not been reported for any MTAN.[8]

Structural comparison of *Vc*MTAN-BuTDIA [Protein Data Bank (PDB) entry 3DP9][9] with *Ec*MTAN-MTDIA (PDB entry 1Y6Q)[7] demonstrated similar overall structures with a root-mean-square deviation (rmsd) of 0.56 Å, in an all-atom comparison, with 2117 atoms accepted for alignment.[10] Previous molecular dynamic simulations of these enzymes in complex with BuTDIA suggested that an increased level of dynamic motion in the *Ec*MTAN complex was responsible for the binding of transition-state analogues being tighter than to *Vc*MTAN.[11] Here, in addition to the mutagenesis analysis, we determined the crystal structures of *Ec*MTAN-BuTDIA (PDB entry 4WKC), *Vc*MTAN-MTDIA (PDB entry 4WKB), and $VcMTAN_{TRIPLE}$-MTDIA (PDB entry 4X24) to permit direct comparisons between MTANs in complexes with the same inhibitors and to probe the effects of multiple mutations on the structures.

We measured the thermodynamic and kinetic properties of *Vc*MTANs with active site residues mutated to be identical to those residues found in *Ec*MTAN. The original hypothesis was that the catalytic site residue differences between *Vc*MTAN and *Ec*MTAN are responsible for the differences in ligand binding affinities and thermodynamic properties. Mutation of the active site residues of *Vc*MTAN to match those of *Ec*MTAN was anticipated to shift the catalytic properties of the modified *Vc*MTANs to more closely resemble those of *Ec*MTAN. Instead, the inhibitor affinity and the thermodynamic binding contributions in the altered *Vc*MTANs became more dissimilar to the properties of *Ec*MTAN. The mutations also altered catalytic site cooperativity, revealing a functional path for dimer−subunit communication in *Vc*MTAN.

MATERIALS AND METHODS

Chemicals. Transition-state analogue inhibitors were synthesized, purified, and characterized as previously reported.[12,13] [^{14}C]MT-DADMe-ImmA [MTDIA*, 4′-deaza-1′-aza-2′-deoxy-1′-(9-[^{14}C]methylene)-Immucillin-A] was synthesized with the incorporation of [^{14}C]formaldehyde to introduce the radiolabel at the methylene bridge.[6]

Enzyme Expression. The *Vc*MTAN (WT) gene, contained in a pDEST14 (Life Technologies) vector, was expressed and the protein purified as previously reported.[6] Mutant *Vc*MTANs were generated using mutagenic polymerase chain reaction (PCR) primers (Life Technologies) and the GENEART Site-Directed Mutagenesis System (Life Technologies). The PCR product was transformed into One Shot TOP10 Electrocomp Cells (Life Technologies) and plated onto LB agar plates containing the appropriate antibiotic. Plasmids from isolated colonies were sequenced across the MTAN region to confirm the presence of the mutation and then transformed into BL21(DE3) competent cells (Life Technologies). Proteins were expressed in cells grown in LB, induced with 1 mM IPTG (37 °C, 10 h), and purified on a Ni-NTA benchtop column according to a previously published protocol.[6] The proteins were >90% pure as assessed by sodium dodecyl sulfate−polyacrylamide gel electrophoresis.

Protein Preparation for ITC. MTANs are copurified with tightly bound adenine, and it was necessary to remove this ligand prior to ITC measurements. Adenine was removed by dialysis against phosphate buffer and activated charcoal as previously described.[6] The dimer concentrations used in ITC experiments ranged from 60 to 120 μM.

Kinetic Analysis. The K_M and k_{cat} values were determined using a modified protocol for a luminescence assay that converts the product adenine to ATP in a coupled assay in which the ATP is detected by luciferase.[14] Each reaction was performed in 50 μL in a 96-well plate format, and luminescence was detected at 570 nm using a SpectraMax L Luminescence Microplate reader (Molecular Devices). Reaction wells contained 50 mM Tris acetate, 1 mM NH_4Cl, 1 mM PEP, 1 mM PRPP (pH 7.7), 8 μL of ATPlite (PerkinElmer), and 10 mM $MgCl_2$. The coupling enzymes pyruvate phosphate dikinase (*Clostridium symbiosum* PPDK,[15] EC 2.7.9.1) and adenine phosphoribosyltransferase (*Saccharomyces cerevisiae* APRTase,[16] EC 2.4.2.7) were added in excess at levels of 320 and 20 microunits/well, respectively. The MTAN concentrations used ranged from 5 to 25 pM. The reactions were

DOI: 10.1021/bi501487w
Biochemistry 2015, 54, 2520−2529

Table 1. Data Collection and Refinement Statistics for *Ec*MTAN·BTDIA and *Vc*MTAN·MTDIA

	*Ec*MTAN-BTDIA	*Vc*MTAN-MTDIA	$Vc\text{MTAN}_{\text{TRIPLE}}$-MTDIA
Data Collection			
space group	$C222_1$	$P2_1$	$P2_1$
no. of molecules in the asymmetric unit	1	2	2
cell dimensions			
a, *b*, *c* (Å)	71.40, 91.39, 70.64	53.19, 72.00, 61.65	52.90, 72.71, 61.62
β (deg)	90	110.3	110.0
resolution (Å)[a]	50.0−1.64 (1.67−1.64)	50.0−1.37 (1.39−1.37)	50.0−1.50 (1.53−1.50)
no. of unique reflections[a]	28677 (1394)	85031 (4510)	69602 (3351)
R_{merge}[a]	0.083 (0.537)	0.048 (0.220)	0.082 (0.685)
$I/\sigma I$[a]	32.9 (4.2)	27.3 (6.8)	18.7 (1.8)
completeness (%)[a]	99.9 (98.3)	93.0 (99.1)	99.1 (96.8)
Refinement			
resolution (Å)	30.0−1.64	30.0−1.37	30.0−1.50
R_{cryst}	0.159	0.164	0.169
R_{free}	0.184	0.183	0.187
rmsd			
bond lengths (Å)	0.008	0.007	0.008
bond angles (deg)	1.37	1.37	1.40
no. of atoms (average *B* factor)			
protein	1735 (17.6)	3579 (13.4)	3544 (17.1)
inhibitor	23 (13.6)	40 (9.1)	40 (12.4)
waters	169 (27.4)	431 (24.3)	360 (26.6)
other	13 (34.4)		10 (43.3)
PDB entry	4WKC	4WKB	4X24

[a]Numbers in parentheses indicate values for the highest-resolution shell.

initiated by the addition of varying concentrations of MTA (0.02−1 μM).

Catalytic Site Titration. MTDIA has a high affinity for native MTANs and therefore exhibits stoichiometric binding in ITC or static preincubation experiments. MTDIA was added to MTAN at known molar ratios and the residual activity recorded to explore catalytic site stoichiometry. A direct UV−vis spectrophotometric assay was used to measure the disappearance of MTA as a function of time at 25 °C and 274 nm.

K_i Determination, Isothermal Titration Calorimetry Studies, and Processing of ITC Data. The experimental procedures for quantitation of kinetic parameters, catalytic site titration, and isothermal titration calorimetry (ITC) for MTAN have been described in detail.[6] The K_i values were determined using varying concentrations of the inhibitor in the presence of 0.8 mM MTA and using 1.0 unit of xanthine oxidase (Sigma-Aldrich), monitored at 305 nm. MTAN concentrations were between 5 and 20 pM. For $Vc\text{MTAN}_{\text{V153I}}$, the k_{cat} is reduced and higher concentrations of enzyme and inhibitor were used to compensate for lower catalytic activity. $Vc\text{MTAN}_{\text{V153I}}$ enzyme activity was unstable in the long assays required for slow-onset K_i measurements, and these values were not obtained.

In brief, ITC studies were conducted using a VP-ITC (MicroCal) microcalorimeter. Inhibitors were dissolved in the dialysate from protein preparation, and all solutions were filtered (Millipore, 0.2 μm) and degassed (Microcal Thermovac) for 15 min. The reference cell was filled with dialysate; 1.5 mL of enzyme was loaded into the sample cell, and 250 μL of the inhibitor solution was loaded into the injection syringe. Titration injection volumes were 5−8 μL. All titrations were conducted at 25 °C. The ITC data were fit to the equations provided in Origin7, which describe two distinct independent binding sites. The K_i* values were used in eq 1 to generate ΔG. ΔH is the integral of the power needed to maintain the temperature of the sample cell at the same temperature as the reference cell after injection. The entropy term was determined using the Gibbs free energy equation (eq 2).

$$\Delta G = RT \ln(K_i^*) \quad (1)$$

$$\Delta G = \Delta H - T\Delta S \quad (2)$$

Titration of MTDIA to MTANs. [^{14}C]MTDIA (MTDIA*) was incubated with the enzyme at varying MTDIA*:MTAN dimer ratios. The quantity of bound MTDIA* was measured after separation with a spin filter (Amicon) that retained enzyme and bound ligand and allowed unbound MTDIA* to pass through the filter. Initial and final MTDIA* concentrations were measured via liquid scintillation counting on a Tricarb 2910 TR instrument (PerkinElmer).

Kinetic Constants for ITC Analysis. ITC titrations for native *Ec*MTAN and *Vc*MTAN with MTDIA were reported previously and used K_i values based on K_M values obtained at high substrate concentrations, corresponding to second-site filling.[6] Here we use the more sensitive luciferase assay at low substrate concentrations that reports on the K_M values at the first catalytic site. Thus, the kinetic and thermodynamic parameters for native *Ec*MTAN and *Vc*MTAN differ from those reported previously.

Crystallization of *E. coli* MTAN-BuTDIA, *V. cholerae* MTAN-MTDIA, and *V. cholerae* $\text{MTAN}_{\text{TRIPLE}}$-MTDIA. Enzymes were concentrated to 10 mg/mL and incubated with 2 equiv of the respective inhibitors. Both proteins were crystallized with the C-terminal TEV cleavage site and His_6 tag intact. All crystallization experiments were performed at 22 °C using the sitting drop vapor diffusion technique. Rod-shaped crystals (0.02 mm × 0.03 mm × 0.27 mm) of *Ec*MTAN-BuTDIA were obtained overnight using 0.2 M ammonium

DOI: 10.1021/bi501487w
Biochemistry 2015, 54, 2520−2529

Table 2. Kinetic Constants for *Vc*MTAN and Mutants Determined Using the Luminescence-Based Assay

MTAN	K_M (nM)	k_{cat} (s^{-1})	k_{cat}/K_M ($\times 10^6$ M^{-1} s^{-1})	$K_{i,MTDIA}$ (pM)	$K_{i,BuTDIA}$ (pM)	K_i (MTDIA/BuTDIA)
*Vc*MTAN						
WT	61 ± 6	0.18 ± 0.01	3.0 ± 0.3	2.7 ± 0.2	0.21 ± 0.04	13
A113P	262 ± 29	0.17 ± 0.01	0.7 ± 0.1	62 ± 7	2.4 ± 0.5	26
V153I	430 ± 47	$(7.9 \pm 4) \times 10^{-3}$	$(1.8 \pm 2) \times 10^{-2}$	NA[a]	NA[a]	NA[a]
DOUBLE	202 ± 23	$(7.4 \pm 3) \times 10^{-2}$	0.4 ± 0.1	3.0 ± 0.5	10.3 ± 1.2	0.3
TRIPLE	536 ± 122	0.11 ± 0.01	0.2 ± 0.1	166 ± 22	3.3 ± 0.5	50
*Ec*MTAN	139 ± 18	0.32 ± 0.01	2.3 ± 0.3	0.16 ± 0.02	0.20 ± 0.04	0.8

[a]Not available.

acetate, 0.1 M BIS-TRIS (pH 5.5), and 25% (w/v) polyethylene glycol 3350. Block-shaped crystals (0.04 mm × 0.16 mm × 0.28 mm) of *Vc*MTAN-MTDIA were obtained over 2 weeks using 0.1 M diammonium hydrogen citrate and 15% (w/v) polyethylene glycol 3350. Rod-shaped crystals (0.03 mm × 0.03 mm × 0.35 mm) of $VcMTAN_{TRIPLE}$-MTDIA were obtained over a week using 0.2 M ammonium chloride (pH 6.3) and 20% (w/v) polyethylene glycol 3350.

Data Collection and Processing. The inhibitor-bound *Ec*MTAN and *Vc*MTAN crystals were transferred to a cryoprotectant solution containing 20% (v/v) glycerol and the respective mother liquors [80% (v/v)] prior to being flash-cooled in liquid nitrogen. Diffraction data for *Ec*MTAN-BuTDIA and *Vc*MTAN-MTDIA crystals were collected with 1.075 Å wavelength radiation at the X29A beamline (Brookhaven National Laboratory, Upton, NY) on an ADSC Q315 CCD X-ray area detector to 1.64 and 1.37 Å resolution, respectively. Diffraction data for $VcMTAN_{TRIPLE}$-MTDIA crystals were collected with 0.9793 Å wavelength radiation at the LRL-CAT beamline (Argonne National Laboratory, Argonne, IL) on a Rayonix 225 HE CCD detector to 1.50 Å resolution. Diffraction intensities were integrated and scaled with Denzo and Scalepack.[17] The diffraction data statistics are summarized in Table 1.

Structure Determination. The structures were determined by molecular replacement with Molrep,[18] using a single monomer from the previously published structures of *Ec*MTAN-MTDIA (PDB entry 1Y6Q) and *Vc*MTAN-BuTDIA (PDB entry 3DP9) as search models. For all structures, the refinement of the initial solution and subsequent refinements were conducted using a restrained refinement performed with Refmac,[19] using all data between 30.0 Å and the respective high-resolution cutoffs. Manual model rebuilding was conducted using Coot.[20] Difference Fourier maps calculated with $F_{obs} - F_{calc}$ coefficients revealed ordered water molecules and strong unambiguous density difference, corresponding to the MTDIA and BuTDIA inhibitors. The coordinates for both inhibitors were present in the Coot monomer library, having monomer codes TDI for MTDIA and BIG for BuTDIA. Water molecules with proper hydrogen bonding coordination and electron densities greater than one rmsd and three rsmds in maps calculated with $2F_{obs} - F_{calc}$ and $F_{obs} - F_{calc}$ coefficients, respectively, were included in the model. For the *Vc*MTAN and $VcMTAN_{TRIPLE}$ structures, all of the *Vc*MTAN residues (residues 1−231) and six of the 13 residues in the cleavage/His_6 tag (residues 232−237) were sufficiently ordered to be included in the model. Likewise for the *Ec*MTAN structure, all residues (residues 1−232) were included in the model; however, none of the residues in the cleavage/His_6 tag could be modeled. Several residues in each structure were modeled with alternate conformations. The *Ec*MTAN-BuTDIA structure was refined to an R_{cryst} of 15.9% and an R_{free} of 18.4%, the *Vc*MTAN-MTDIA structure to an R_{cryst} of 16.5% and an R_{free} of 18.3%, and the $VcMTAN_{TRIPLE}$-MTDIA structure to an R_{cryst} of 16.9% and an R_{free} of 18.7%. Analysis of the structures in Coot revealed good stereochemistry with no residues falling into the disallowed regions of the Ramachandran plot in either of the *Vc*MTAN structures and one outlier in the *Ec*MTAN structure (Ser155). The refinement statistics are listed in Table 1.

RESULTS

Structural Similarity between *Vc*MTAN and *Ec*MTAN. The crystal structures reported here permit direct comparison of the *Ec*- and *Vc*MTANs bound to the transition-state inhibitors MTDIA and BuTDIA. All four inhibitor-bound proteins are structurally similar. The overall rmsd between an all-atom comparison of *Vc*MTAN and *Ec*MTAN in complex with MTDIA is 0.57 Å (2541 atoms accepted for comparison), and the same comparison for the complexes with BuTDIA is 0.61 Å (2495 atoms accepted for comparison). The overall rmsd between an all-atom comparison of $VcMTAN_{TRIPLE}$ and *Ec*MTAN in complex with MTDIA is 0.54 Å (2539 atoms). The conformations of residues at positions 113, 153, and 158 in *Vc*MTAN and analogous positions in *Ec*MTAN are highlighted in Figure 1, where *Vc*MTAN residues (blue) are overlaid with *Ec*MTAN residues (green). The transition-state analogues are colored according to the active site in which they are bound.

The hydrogen bonding distances and hydrophobic interactions to bound inhibitors are similar between *Vc*MTAN and *Ec*MTAN (Figure S3 of the Supporting Information). Five key hydrogen bonds to the inhibitors are found in all five structures: Ile152/Val153 to N1 and N6, Asp197/198 to N6 and N7, and inhibitor N1′ to the nucleophilic water molecule. Additionally, Phe151/152 participates in π-stacking interactions with the deazapurine moiety, having centroid−centroid distances of ∼4.4 ± 0.2 Å (Figure S4 of the Supporting Information). A related interaction is observed in purine nucleoside phosphorylase (PNP), where Phe200 shares a related interaction with 9-deazahypoxanthine from transition-state analogues bound in the catalytic sites.[21,22]

Hydrophobic interactions involving the 5′-alkyl chains of MTDIA and BuTDIA are similar in all five structures, despite the increased steric bulk of Pro113 in *Vc*MTAN compared to that of Ala113 in *Ec*MTAN. The distances between hydrophobic interactions vary between 4.1 and 4.9 Å in the BuTDIA-bound structures and between 4.5 and 4.7 Å in the MTDIA-bound structures (Figure S3 of the Supporting Information). Overall, the position and conformations of MTDIA and BuTDIA bound to *Ec*- and *Vc*MTAN are nearly superimposable with respect to their binding sites, with only the 5′-butyl chains varying in orientation (Figure S6 of the Supporting Information).

DOI: 10.1021/bi501487w
Biochemistry 2015, 54, 2520−2529

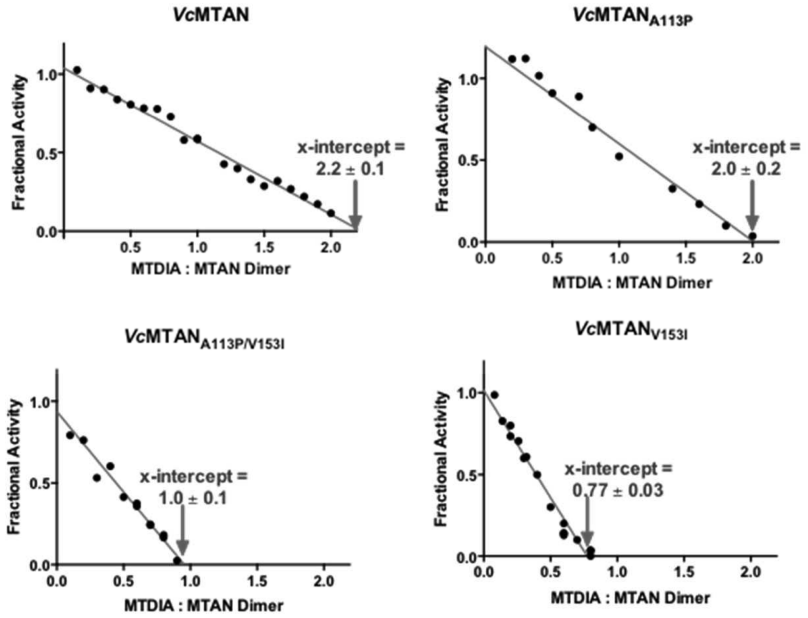

Figure 2. Fractional activity of the MTAN homodimer following titration with the tight binding inhibitor MTDIA. Wild-type *Vc*MTAN and *Vc*MTAN$_{A113P}$ require two inhibitor molecules to be bound per homodimer to abolish MTAN activity. *Vc*MTAN$_{V153I}$ and *Vc*MTAN$_{A113P/V153I}$ require one inhibitor molecule bound per homodimer to abolish activity.

As mentioned above, Arg158 is near Val153 in *Vc*MTAN, whereas Gly157 and Ile152 form this comparable pair in *Ec*MTAN. Static modeling of the respective structures suggested that *Vc*MTAN$_{V153I}$ might have side chain clashes with Arg158 (Figure S4 of the Supporting Information). Given this observation and the large change in side chain volume, a Arg158Gly mutant was also investigated in *Vc*MTAN.

Steady-State Kinetic Properties. The sensitivity of the luminescence assay for MTAN activity permitted determination of the nanomolar K_M value for first-catalytic site filling in MTANs (Table 2 and Figure S7 of the Supporting Information). The affinity of *Vc*MTAN for MTA (61 nM) is greater than the affinity of *Ec*MTAN for MTA (139 nM), while the catalytic efficiencies are similar at 2.3 or 3.0 × 10^6 M^{-1} s^{-1} (Table 2). The K_M values for *Vc*MTAN$_{A113P}$ and *Vc*MTAN$_{A113P/V153I}$ (*Vc*MTAN$_{DOUBLE}$) mutants are similar (262 and 202 nM, respectively) but are increased to 430 nM for *Vc*MTAN$_{V153I}$. The k_{cat} values were unchanged in *Vc*MTAN$_{A113P}$ and decreased 22-fold in *Vc*MTAN$_{V153I}$ (Table 2). In *Vc*MTAN$_{DOUBLE}$, a fraction of the substrate affinity was restored (improved K_M) and the catalytic efficiency improved 20-fold compared to that of *Vc*MTAN$_{V153I}$. *Vc*MTAN$_{A113P/V153I/R158G}$ (*Vc*MTAN$_{TRIPLE}$) most closely resembles the catalytic site of *Ec*MTAN, yet its K_M value is significantly increased. None of the *Vc*MTANs mutated toward *Ec*MTAN displayed catalytic efficiencies approaching that of *Ec*MTAN.

Dissociation Constants for Transition-State Analogues with *Ec*MTAN and *Vc*MTANs. Single and combined mutations in *Vc*MTAN at positions 113, 153, and 158 altered the dissociation constants for MTDIA and BuTDIA (Table 2). The K_i value for MTDIA is 6 times larger for *Vc*MTAN than for *Ec*MTAN, and the K_i values for BuTDIA are similar for both enzymes. Increasing the 5′-alkyl chain length from methyl (MTDIA) to butyl (BuTDIA) has little effect on *Ec*MTAN but results in a 13-fold change for *Vc*MTAN. *Vc*MTAN$_{DOUBLE}$ has a K_i similar to that of the native enzyme for MTDIA, despite its reduced K_M value. The K_i values for MTDIA are increased in the A113P mutant and further increased in the triple mutant. *Vc*MTAN mutants exhibited increased K_i values for BuTDIA in all mutants tested compared to those of its parent.

A Conservative Active Site Mutation Affects Cooperativity. Catalytic site titrations of *Vc*MTANs with MTDIA reveal that both active sites of *Vc*MTAN and *Vc*MTAN$_{A113P}$ must be filled with inhibitor to cause complete catalytic inhibition (Figure 2). In contrast, inhibitor bound to one active site of either *Vc*MTAN$_{V153I}$ or *Vc*MTAN$_{DOUBLE}$ causes complete inhibition (Figure 2). Native and mutant *Vc*MTANs migrated the same on nondenaturing gels (Figure S8 of the Supporting Information). Thus, altered quaternary structure in either *Vc*MTAN$_{DOUBLE}$ or *Vc*MTAN$_{V153I}$ is unlikely to account for the half-the-sites inhibition. Complete inhibition of dimeric mutant MTANs by inhibitor binding to a single monomer raises the question of inhibitor binding to the second catalytic site. MTDIA* titrations sufficient to saturate one or two catalytic sites of *Vc*MTAN and *Vc*MTAN$_{A113P}$ showed complete binding at the first site and near-stoichiometric binding at the second site. Thus, both sites bind inhibitor in stoichiometric titrations, but binding to the second active site is weaker than binding to the first (Figure 3). In *Vc*MTAN$_{DOUBLE}$ and *Vc*MTAN$_{V153I}$, titration to two MTDIA* molecules per dimer left more MTDIA* unbound as both the first and second sites were titrated (Figure 3). *Vc*MTAN$_{DOUBLE}$ and *Vc*MTAN$_{V153I}$ bind inhibitor less well at both the first active and second catalytic sites than *Vc*MTAN or *Vc*MTAN$_{A113P}$.

Isothermal Calorimetry of the Transition-State Analogue Binding to Mutant *Vc*MTANs. Isothermal calorimetry (ITC) experiments measure distinct energetic contributions to inhibitor binding. Enthalpic changes occurred as both catalytic sites were filled in *Vc*MTAN and *Vc*MTAN$_{A113P}$, but only for first-site filling with V153I, DOUBLE, and TRIPLE mutants (Table 3). Plotting the isotherms together emphasizes the differences in the energetics of binding to the *Vc*MTANs (Figure 4B).

DOI: 10.1021/bi501487w
Biochemistry 2015, 54, 2520−2529

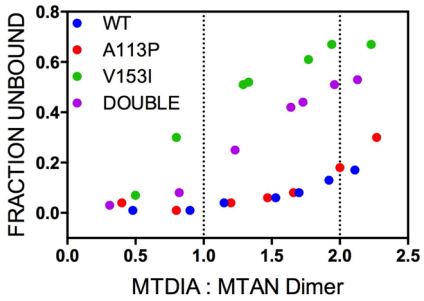

Figure 3. Fraction of unbound radiolabeled MTDIA as a function of dimer catalytic site titration in native (WT) or mutated *Vc*MTANs (A113P, V153I, and DOUBLE). Fraction of MTDIA unbound (*y*-axis) following titration of the MTAN dimer with varying concentrations of MTDIA (*x*-axis). An MTDIA:MTAN dimer value of 1 indicates sufficient inhibitor to fill one of the two catalytic sites. An MTDIA:MTAN dimer value of 2 indicates an inhibitor stoichiometry that can fill both catalytic sites, if the affinity is high. MTAN dimer concentrations were 27−33 μM for all experiments except for WT, for which the concentrations were 27−85 μM.

Table 3. Thermodynamic Constants for Binding of MTDIA to Wild-Type and Mutant *Vc*MTANs

MTAN + MTDIA titrant pair	site[a]	ΔG^b (kcal mol^{-1})	ΔH^c (kcal mol^{-1})	$T\Delta S^d$ (kcal mol^{-1})
Vc-WT	first	−15.8 ± 0.1	−6.0 ± 0.2	−9.8 ± 0.2
	second	−14.3 ± 0.2	−2.6 ± 0.3	−11.7 ± 0.4
Vc-A113P	first	−13.9 ± 0.1	−2.9 ± 0.1	−11.0 ± 0.1
	second	−13.5 ± 0.8	−1.8 ± 0.2	−11.7 ± 0.8
Vc-V153I	single	−10.6 ± 0.2	−4.9 ± 0.1	−5.7 ± 0.2
Vc-DOUBLE	single	−15.7 ± 0.1	−3.9 ± 0.1	−11.8 ± 0.1
Vc-TRIPLE	single	−13.3 ± 0.1	−4.8 ± 0.2	−8.5 ± 0.2
Ec-WT	first	−17.4 ± 0.9	−18.9 ± 0.2	1.5 ± 0.9
	second	−10.2 ± 0.1	−16.8 ± 0.2	6.6 ± 0.2

[a]Site represents which dimer site contributed most to the indicated enthalpic and associated thermodynamic properties using the best fit described in Materials and Methods (each monomer of the dimer has a single active site). Single indicates only the first site has an enthalpic signature as detected by ITC. [b]ΔG was calculated from the K_i* (Table 1) using the equation $\Delta G = RT \ln K_i$*. [c]ΔH was determined from the ITC titrations of enzyme with inhibitor for each of the two catalytic site of the enzyme dimer. [d]$-T\Delta S$ was calculated from the Gibbs free energy equation.

The enthalpic isotherm generated for binding of MTDIA to *Vc*MTAN indicated negative cooperativity. As inhibitor filled the second catalytic site the heat released by the system decreased (Figure 4A). Isotherms for *Vc*MTAN-MTDIA and $Vc\text{MTAN}_{A113P}$-MTDIA are similar and end with an abrupt loss of heat production when catalytic site stoichiometry is reached, as expected for tight-binding inhibitors. The enthalpy generated in $Vc\text{MTAN}_{A113P}$ is 3 kcal mol^{-1} less favorable than the enthalpy generated from its parent. The enthalpies generated by $Vc\text{MTAN}_{DOUBLE}$, $Vc\text{MTAN}_{TRIPLE}$, and $Vc\text{MTAN}_{V153I}$ are more favorable than that of $Vc\text{MTAN}_{A113P}$ by −1.0, −1.9, and −2.0 kcal mol^{-1}, respectively. Thus, all *Vc*MTAN catalytic site changes toward *Ec*MTAN resulted in unfavorable enthalpy contributions to MTDIA binding compared to that of native *Vc*MTAN (Figure 5).

In contrast to the unfavorable enthalpic changes, $Vc\text{MTAN}_{A113P}$ and $Vc\text{MTAN}_{DOUBLE}$ displayed favorable entropic gains while $Vc\text{MTAN}_{V153I}$ and $Vc\text{MTAN}_{TRIPLE}$ displayed entropic penalties compared to native *Vc*MTAN (Figure 5). The entropic gains with $Vc\text{MTAN}_{A113P}$ and $Vc\text{MTAN}_{DOUBLE}$ were overcome by an even larger enthalpic penalty compared to that of *Vc*MTAN.

Potential Origins for Altered Thermodynamic Parameters. We explored if the changes in binding thermodynamics might be attributed to alterations in the active site water reorganization or hydrophobicity due to altered active site volumes. Comparison of the cavities of *Vc*MTAN, *Ec*MTAN, and $Vc\text{MTAN}_{TRIPLE}$ indicated that the cavity volumes of $Vc\text{MTAN}_{TRIPLE}$ at the active sites (both A and B subunits) remained unchanged, while the cavity volume located at the dimer interface increased in $Vc\text{MTAN}_{TRIPLE}$ (Figure S9 of the Supporting Information). The cavity volumes of active site A and active site B are similar between *Vc*MTAN and $Vc\text{MTAN}_{TRIPLE}$ with a <3% variation in volume. The active site volumes of $Vc\text{MTAN}_{TRIPLE}$ are 18% (monomer A) and 6% (monomer B) smaller than that of *Ec*MTAN (Table 4). The most striking difference occurs at the dimer interface of $Vc\text{MTAN}_{TRIPLE}$, where the cavity volumes are increased 1.9- and 2.2-fold relative to those of *Vc*MTAN and *Ec*MTAN, respectively (Table 4). This doubling of cavity volume at the dimer interface in $Vc\text{MTAN}_{TRIPLE}$ suggests a possible mechanism for the disruption of catalytic site cooperativity. The similar catalytic site volumes make it less likely that changes in solvent access to the catalytic sites are responsible for altered thermodynamics.

DISCUSSION

Mutations toward Catalytic Site Similarity. Attempts to convert the catalytic site of *Vc*MTAN in terms of sequence and structural identity to those of *Ec*MTAN led to catalytic dysfunction. The Val153Ile mutation caused *Vc*MTAN to acquire half-the-sites inhibitor susceptibility. Thus, the Val153 region is involved in facilitating catalytic communication between *Vc*MTAN monomers. Although large effects due to conservative mutations are surprising, they are documented in other systems, including dihydrofolate reductase (DHFR). *E. coli* DHFR (*Ec*DHFR) catalyzes the reduction of 7,8-dihydrofolate (DHF) to 5,6,7,8-tetrahydrofolate (THF). In the active site, a conservative residue change of Asp27Glu, to mimic the Glu at this position in the human enzyme (Glu31), affects catalysis, producing a similar k_{cat}; however, the $K_{M(DHF)}$ is increased 20-fold, and methotrexate affinity is decreased 176-fold.[23,24] Asp27 exhibits this effect through an intervening water molecule required for proton transfer.[25,26] The presence of Glu31 in *h*DHFR is proposed to alter enzyme dynamics, which is linked to differences in catalytic properties and metabolic flux between *Ec*DHFR and *h*DHFR.[27]

Possible Path for Cooperativity. The Val153Ile mutation in the *Vc*MTANs gives rise to half-the-sites inhibition, with inhibitor binding at one site inhibiting catalysis at both sites. The protein connectivity among the catalytic sites of *Ec*MTAN, *Vc*MTAN, and $Vc\text{MTAN}_{TRIPLE}$ by the most direct route includes His98, Asp99, Gly149, Asp150, Ala151, and Phe152 (yellow) and to a lesser extent Ala100, Asp101, and Val102 (Figure 6, blue). These residues are conserved between the *Ec*- and *Vc*MTANs and are highly similar in all of the structures, with a rmsd for the Cα peptide atoms of 0.162 Å between the *Ec*- and *Vc*MTANs and 0.143 Å between *Ec*- and $Vc\text{MTAN}_{TRIPLE}$. From this analysis, there is no obvious structural reason for the change from independent active sites to half-the-sites reactivity. However, the kinetic analysis makes

DOI: 10.1021/bi501487w
Biochemistry 2015, 54, 2520−2529

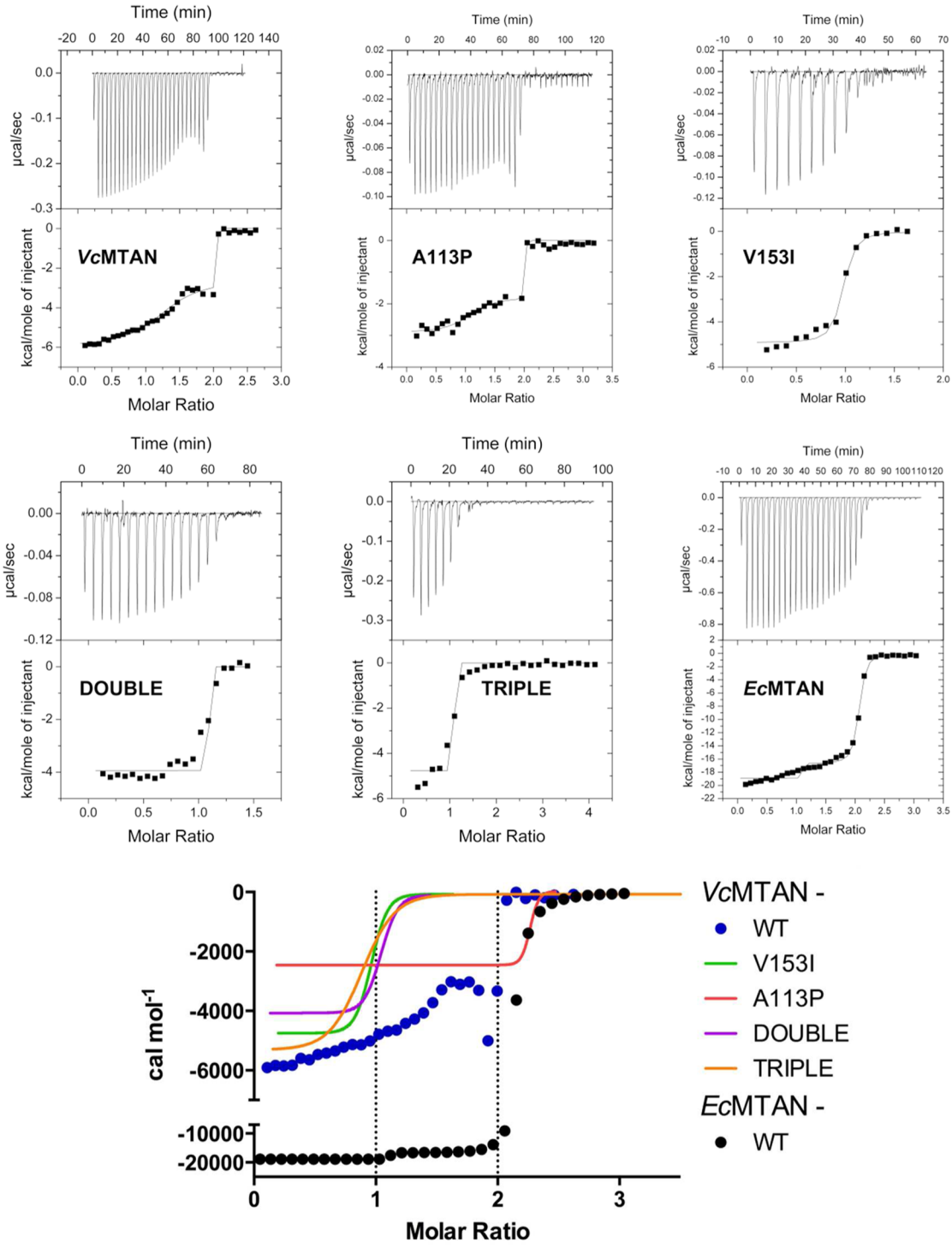

Figure 4. Comparison of heat isotherms for titration of MTDIA against *Vc*MTAN (WT and mutants) (top six panels). In the bottom panel, the energetics are shown on a common scale to emphasize the difference between the systems.

it clear that in the Val153Ile mutant, the second site is rendered catalytically nonfunctional by inhibitor binding at only one site.

Mutations in Groups. *Vc*MTAN$_{TRIPLE}$ is the mutant most closely related to *Ec*MTAN, but the changes resulting in a catalytic site that is more similar to that of *Ec*MTAN cause K_M, k_{cat}, and inhibitor binding to be less efficient than those of the parent *Vc*MTAN and make it even less like *Ec*MTAN. These changes occur without any significant changes in the overall protein structure of the triple mutant. Although catalytic site function is impaired in *Vc*MTAN$_{V153I}$, the combination of Val153Ile with Ala113Pro partly restores inhibitor and substrate binding. However, this second mutation is insufficient to restore catalytic independence at the active sites or improve the catalytic properties toward those of *Ec*MTAN.

With *Vc*MTAN$_{V153I}$ as the reference point, changes toward an active site that is more similar to the active site of *Ec*MTAN result in enthalpic gains in inhibitor binding but are offset by larger entropic penalties. The evolution of the Ala113-Val153-Arg158 sites in *Vc*MTAN appears to be group-dependent. Thus, perturbation of any member of the group results in a loss

DOI: 10.1021/bi501487w
Biochemistry 2015, 54, 2520−2529

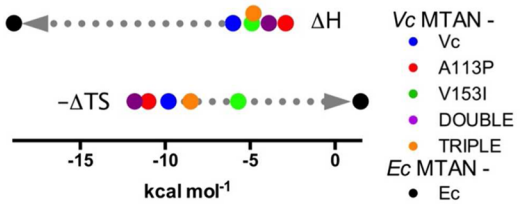

Figure 5. Representation of the ΔH and $-T\Delta S$ values for binding of MTDIA to *Ec*MTAN, *Vc*MTAN, and *Vc*MTAN mutants at 25 °C. The gray dotted arrow indicates the direction either ΔH or $-T\Delta S$ must shift for the energetic binding profile of the *Vc*MTAN mutants to more closely match that of *Ec*MTAN.

Table 4. Cavity Volumes of *Vc*MTAN$_{TRIPLE}$, *Vc*MTAN, and *Ec*MTAN at Monomer A, Monomer B, and the Dimer Interface[a]

	volume (Å^3)		
	monomer A	monomer B	dimer interface
*Vc*MTAN$_{TRIPLE}$	185.0	185.3	1028.4
*Vc*MTAN	180.4	181.0	543.2
*Ec*MTAN	224.3	197.4	478.2

[a]Volumes calculated using a 2.5 Å query diameter on CASTp.

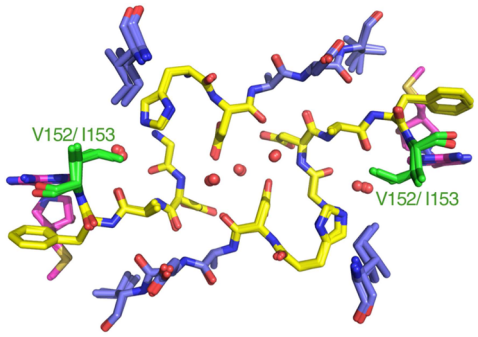

Figure 6. Stick figure of *Ec*MTAN, *Vc*MTAN, and *Vc*MTAN$_{TRIPLE}$ MTANs with MTDIA bound, illustrating connectivity between active sites. The transition-state analogue MTDIA is colored in magenta. The residues at position 153 are colored green. Amino acids in a direct route between active sites are colored yellow, whereas those more distal are colored blue.

of catalytic fitness. Execution of a Basic Local Alignment Search Tool (BLAST) with wild-type *Vc*MTAN as the query sequence indicates that the Ala113-Val153-Arg158 sites and Ala-Val-Xxx (Xxx represents a variable amino acid) sites are exclusively present in the family Vibrionaceae. In contrast, the corresponding sites are Pro-Ile-Gly in *Ec*MTAN, and this sequence is present exclusively in the Enterobacteriaceae family, with its members belonging to the genera *Escherichia*, *Salmonella*, and *Citrobacter* (Figure S10 of the Supporting Information).[28] The corresponding Pro-Ile-Xxx residues are found across multiple species of the Gram-positive firmicutes and the Gram-negative α-proteobacteria, δ-proteobacteria, ε-proteobacteria, and γ-proteobacteria (Figure S10 of the Supporting Information). The Ala-Val-Xxx and Pro-Ile-Xxx groups apparently co-evolved with a complementary protein scaffold. Simply altering the catalytic site groups in *Vc*MTAN without altering the protein architectural scaffold causes a decrease in catalytic and binding functions.

Similar Overall Structures between Enzymes. Comparing complexes of MTDIA or BuTDIA bound to either MTAN shows that different inhibitors cause small rmsds in the complexes, 0.35 and 0.21 Å for *Ec*MTAN and *Vc*MTAN, respectively. Additionally, the rmsds between the *Ec*MTAN and *Vc*MTAN proteins bound to MTDIA or BuTDIA are also small, 0.57 and 0.60 Å, respectively. Taken together, significantly different conformational geometries are unlikely to account for differences in inhibitor affinity for these enzymes. The active site of the *Vc*MTAN$_{TRIPLE}$ mutant is nearly identical to that of *Ec*MTAN (*Ec*MTAN and *Vc*MTAN$_{TRIPLE}$ bound to MTDIA shown in Figure 7). Bound MTDIA overlaps from structures in both enzymes, and both show geometry consistent with the sp^3-hybridized N1′ that acts as the cationic mimic of the C1′ ribocation of the transition state. A single exception to the close structural similarity occurs at Phe105 with a 30° rotation of the phenyl ring. Phe105 is found on the loop of the adjacent monomer, which occludes the active site entrance and might play a role in stabilizing the inhibitor deazapurine ring in the active site (Figure 7). The absence of active site differences between *Vc*MTAN$_{TRIPLE}$ and *Ec*MTAN therefore implicates whole protein dynamic contributions to account for the differences in catalytic properties.

Enzyme Flexibility: Perturbations in Short Time Scale Motions. Molecular dynamics (MD) simulations of apo and BuTDIA-bound *Vc*MTAN and *Ec*MTAN have suggested that the *Ec*MTAN complex retains more Cα dynamic motion than the *Vc*MTAN complex.[11] The increased flexibility was invoked to explain differential inhibitor affinities of BuTDIA for *Ec*MTAN and *Vc*MTAN, as retained system dynamics upon inhibitor binding decreases entropic loss in the bound complex. The average total numbers of hydrogen bonds between *Vc*MTAN and *Ec*MTAN and their bound BuTDIA ligand were similar at 12.85 and 12.45, respectively, suggesting system dynamic contributions beyond catalytic site contacts.[11]

Other Examples of Catalytic Site Connectivity. Examples in which modifications to regions distinct from the active site affect catalytic properties are commonplace in enzymology. In one such example, exhaustive mutagenesis performed in a 110-residue ribonuclease barnase indicated that substitutions at only 15 of 109 positions were not well tolerated. Furthermore, 12 of those 15 critical substitution-sensitive positions did not directly interact with the substrate.[27] In another study, a hybrid β-lactamase (TEM-1), which differed from the parent only at the C-terminus, resulted in an inactive protein despite the C-terminus being distinct from the active site and poorly conserved.[28] These examples provide support that residues apart from the active site can be deterministic in key aspects of the catalytic cycle.

Ec- and *Vc*MTANs possess similar overall protein architecture but small catalytic site differences. By mutationally matching the catalytic site sequences of *Vc*MTAN to that of *Ec*MTAN, we attempted to equalize catalytic site function, but the catalytic properties became even more disparate. The results establish the significance of remote interactions to create catalytic function at sites with the same crystallographic contacts with reactants. The evolutionary distance between *Ec*- and *Vc*MTANs has resulted in drift in both the catalytic sites and the remote protein architecture, working together to optimize the protein architecture−catalytic site interplay. Altering the catalytic site without the overall dynamic architecture solves only part of the evolutionary difference. Clearly, catalytic site sequence design alone will be insufficient to design and engineer efficient enzymatic catalysts. Incorpo-

DOI: 10.1021/bi501487w
Biochemistry 2015, 54, 2520−2529

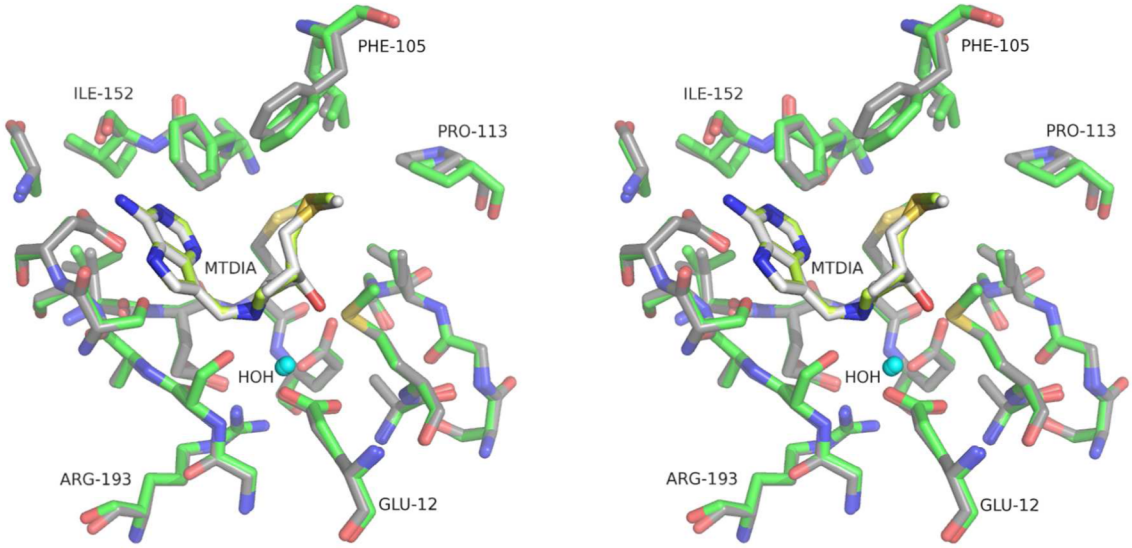

Figure 7. Structural comparison (stereoview) of the active sites of *Ec*MTAN (green) vs $Vc\text{MTAN}_{\text{TRIPLE}}$ (gray) with transition-state analogue MTDIA and a nucleophilic water molecule bound.

ration of appropriate catalytic site functionality requires the appropriate dynamic architecture.[29−31]

CONCLUSIONS

$Vc\text{MTAN}_{\text{DOUBLE}}$ and *Ec*MTAN share 100% active site residue identity, yet considerable differences in kinetic properties were observed. There is a 6-fold decrease in catalytic efficiency and a 20−50-fold decrease in transition-state analogue affinities in $Vc\text{MTAN}_{\text{DOUBLE}}$, despite having matched all inhibitor-interacting active site residues to those identified in *Ec*MTAN. The $Vc\text{MTAN}_{\text{DOUBLE}}$ mutant also became more dissimilar to *Ec*MTAN in thermodynamic terms. Although $Vc\text{MTAN}_{\text{DOUBLE}}$ did not become more similar to *Ec*MTAN, it displayed improved affinity for MTA compared to that of $Vc\text{MTAN}_{\text{V153I}}$ and displayed improved binding to the transition-state analogues relative to the binding of either of the single mutants ($Vc\text{MTAN}_{\text{V153I}}$ or $Vc\text{MTAN}_{\text{A113P}}$).

The presence of the Val153Ile mutation disrupted catalysis at the second active site of the homodimer when the first site was inhibited. Val153 is not located at the dimer interface, nor is it sufficiently close to another residue from the second monomer to exert direct influence on its neighbor. Val153 is likely to be involved in a network of residues involved in facilitating conformational interactions between monomers.

Alterations remote from the catalytic site impose strong catalytic function on similar catalytic sites and thus make design of *de novo* enzymes a difficult goal. Dynamic motions remote from the catalytic site are likely responsible for differences in binding and catalytic properties of the MTANs investigated here. Full protein scaffold dynamical motions are critical for optimized functioning of the MTANs and likely other enzymes. The results reported here, and related work, add growing support to the position that dynamical motions are integral to catalysis.[29,32−34]

ASSOCIATED CONTENT

Supporting Information

Sequence alignment of *E. coli* and *V. cholerae* MTANs, generated using ClustalW2 (Figure S1); the two-dimensional map showing bonding interactions between *Ec*MTAN-MTDIA and *Vc*MTAN-BuTDIA (Figure S2); distances between residues selected for mutation and the bound inhibitor (Figure S3); offset π stacking interaction between *Ec*MTAN and *Vc*MTAN and MTDIA or BuTDIA (Figure S4); structure of static *in silico* mutagenized residues in *Vc*MTAN complexed with BuTDIA (Figure S5); comparison of the bound inhibitor orientation (Figure S6); K_M curves obtained from luciferase-based assay for WT *Vc*MTAN and its mutants and *Ec*MTAN (Figure S7); nondenaturing gel of *Vc*MTAN native and mutant proteins (Figure S8); structural representation of cavity volumes in *Vc*MTAN (Figure S9); and an evolutionary tree with *Vc*MTAN as the query sequence (Figure S10). This material is available free of charge via the Internet at http://pubs.acs.org.

AUTHOR INFORMATION

Corresponding Author

*E-mail: vern.schramm@einstein.yu.edu. Telephone: (718) 430-2813. Fax: (718) 430-8565.

Funding

This research was funded by National Institutes of Health Grants GM41916, GM068036 and The Price Family Foundation, Inc. Financial support for crystallography comes principally from the Offices of Biological and Environmental Research and of Basic Energy Sciences of the U.S. Department of Energy and from the National Center for Research Resources (P41RR012408) and the National Institute of General Medical Sciences (P41GM103473) of the National Institutes of Health.

Notes

The authors declare no competing financial interest.

ACKNOWLEDGMENTS

Data for this study of crystallographic structures were measured at beamline X29A of the National Synchrotron Light Source. Use of the Advanced Photon Source, an Office of Science User Facility operated for the U.S. Department of Energy (DOE) Office of Science by Argonne National Laboratory, was supported by the U.S. DOE under Contract DE-AC02-06CH11357. Use of the Lilly Research Laboratories Collabo-

DOI: 10.1021/bi501487w
Biochemistry 2015, 54, 2520−2529

rative Access Team (LRL-CAT) beamline at Sector 31 of the Advanced Photon Source was provided by Eli Lilly Co., which operates the facility.

■ ABBREVIATIONS

MTAN, 5′-methylthioadenosine/*S*-adenosyl-L-homocysteine nucleosidase; MTA, 5′-methylthioadenosine; MTR, 5′-methylthioribose; *Vc*MTAN, *V. cholerae* MTAN; *Ec*MTAN, *E. coli* MTAN; DADMe-ImmA, 4′-deaza-1′-aza-2′-deoxy-1′-(9-methylene)-Immucillin-A; rmsd, root-mean-square deviation.

■ REFERENCES

(1) Duerre, J. A. (1962) A hydrolytic nucleosidase acting on *S*-adenosylhomocysteine and on 5′-methylthioadenosine. *J. Biol. Chem. 237*, 3737−3741.
(2) Naik, V., and Mahajan, G. (2013) Quorum sensing: A non-conventional target for antibiotic discovery. *Nat. Prod. Commun. 8*, 1455−1458.
(3) Hiratsuka, T., Furihata, K., Ishikawa, J., Yamashita, H., Itoh, N., Seto, H., and Dairi, T. (2008) An alternative menaquinone biosynthetic pathway operating in microorganisms. *Science 321*, 1670−1673.
(4) Li, X., Apel, D., Gaynor, E. C., and Tanner, M. E. (2011) 5′-Methylthioadenosine nucleosidase is implicated in playing a key role in a modified futalosine pathway for menaquinone biosynthesis in *Campylobacter jejuni*. *J. Biol. Chem. 286*, 19392−19398.
(5) Wang, S., Haapalainen, A. M., Yan, F., Du, Q., Tyler, P. C., Evans, G. B., Rinaldo-Matthis, A., Brown, R. L., Norris, G. E., Almo, S. C., and Schramm, V. L. (2012) A picomolar transition state analogue inhibitor of MTAN as a specific antibiotic for *Helicobacter pylori*. *Biochemistry 51*, 6892−6894.
(6) Thomas, K., Haapalainen, A. M., Burgos, E. S., Evans, G. B., Tyler, P. C., Gulab, S., Guan, R., and Schramm, V. L. (2012) Femtomolar inhibitors bind to 5′-methylthioadenosine nucleosidases with favorable enthalpy and entropy. *Biochemistry 51*, 7541−7550.
(7) Lee, J. E., Singh, V., Evans, G. B., Tyler, P. C., Furneaux, R. H., Cornell, K. A., Riscoe, M. K., Schramm, V. L., and Howell, P. L. (2005) Structural rationale for the affinity of pico- and femtomolar transition state analogues of *Escherichia coli* 5′-methylthioadenosine/*S*-adenosylhomocysteine nucleosidase. *J. Biol. Chem. 280*, 18274−18282.
(8) Lee, J. E., Luong, W., Huang, D. J., Cornell, K. A., Riscoe, M. K., and Howell, P. L. (2005) Mutational analysis of a nucleosidase involved in quorum-sensing autoinducer-2 biosynthesis. *Biochemistry 44*, 11049−11057.
(9) Gutierrez, J. A., Crowder, T., Rinaldo-Matthis, A., Ho, M. C., Almo, S. C., and Schramm, V. L. (2009) Transition state analogs of 5′-methylthioadenosine nucleosidase disrupt quorum sensing. *Nat. Chem. Biol. 5*, 251−257.
(10) (2010) *The Pymol molecular graphics system*, version 1.3, Schrödinger, LLC, Portland, OR.
(11) Motley, M. W., Schramm, V. L., and Schwartz, S. D. (2013) Conformational freedom in tight binding enzymatic transition-state analogues. *J. Phys. Chem. B 117*, 9591−9597.
(12) Evans, G. B., Furneaux, R. H., Lenz, D. H., Painter, G. F., Schramm, V. L., Singh, V., and Tyler, P. C. (2005) Second generation transition state analogue inhibitors of human 5′-methylthioadenosine phosphorylase. *J. Med. Chem. 48*, 4679−4689.
(13) Evans, G. B., Furneaux, R. H., Schramm, V. L., Singh, V., and Tyler, P. C. (2004) Targeting the polyamine pathway with transition-state analogue inhibitors of 5′-methylthioadenosine phosphorylase. *J. Med. Chem. 47*, 3275−3281.
(14) Wang, S., Thomas, K., and Schramm, V. L. (2014) Catalytic site cooperativity in dimeric methylthioadenosine nucleosidase. *Biochemistry 53*, 1527−1535.
(15) Wang, H. C., Ciskanik, L., Dunaway-Mariano, D., Von der Saal, W., and Villafranca, J. J. (1988) Investigations of the partial reactions catalyzed by pyruvate phosphate dikinase. *Biochemistry 27*, 625−633.
(16) Shi, W., Tanaka, K. S., Crother, T. R., Taylor, M. W., Almo, S. C., and Schramm, V. L. (2001) Structural analysis of adenine phosphoribosyltransferase from *Saccharomyces cerevisiae*. *Biochemistry 40*, 10800−10809.
(17) Otwinowski, Z., and Minor, W. (1997) Processing of X-ray diffraction data collected in oscillation mode. *Methods Enzymol. 276*, 307−326.
(18) Vagin, A., and Teplyakov, A. (1997) Molrep: An automated program for molecular replacement. *J. Appl. Crystallogr. 30*, 1022−1025.
(19) Murshudov, G. N., Skubak, P., Lebedev, A. A., Pannu, N. S., Steiner, R. A., Nicholls, R. A., Winn, M. D., Long, F., and Vagin, A. A. (2011) Refmac5 for the refinement of macromolecular crystal structures. *Acta Crystallogr. D67*, 355−367.
(20) Emsley, P., Lohkamp, B., Scott, W. G., and Cowtan, K. (2010) Features and development of coot. *Acta Crystallogr. D66*, 486−501.
(21) Antoniou, D., Ge, X., Schramm, V. L., and Schwartz, S. D. (2012) Mass modulation of protein dynamics associated with barrier crossing in purine nucleoside phosphorylase. *J. Phys. Chem. Lett. 3*, 3538−3544.
(22) Saen-Oon, S., Ghanem, M., Schramm, V. L., and Schwartz, S. D. (2008) Remote mutations and active site dynamics correlate with catalytic properties of purine nucleoside phosphorylase. *Biophys. J. 94*, 4078−4088.
(23) Matthews, D., Alden, R., Bolin, J., Freer, S., Hamlin, R., Xuong, N., Kraut, J., Poe, M., Williams, M., and Hoogsteen, K. (1977) Dihydrofolate reductase: X-ray structure of the binary complex with methotrexate. *Science 197*, 452−455.
(24) David, C. L., Howell, E. E., Farnum, M. F., Villafranca, J. E., Oatley, S. J., and Kraut, J. (1992) Structure and function of alternative proton-relay mutants of dihydrofolate reductase. *Biochemistry 31*, 9813−9822.
(25) Fierke, C. A., Johnson, K. A., and Benkovic, S. J. (1987) Construction and evaluation of the kinetic scheme associated with dihydrofolate reductase from *Escherichia coli*. *Biochemistry 26*, 4085−4092.
(26) Deng, H., and Callender, R. (1998) Structure of dihydrofolate when bound to dihydrofolate reductase. *J. Am. Chem. Soc. 120*, 7730−7737.
(27) Bhabha, G., Ekiert, D. C., Jennewein, M., Zmasek, C. M., Tuttle, L. M., Kroon, G., Dyson, H. J., Godzik, A., Wilson, I. A., and Wright, P. E. (2013) Divergent evolution of protein conformational dynamics in dihydrofolate reductase. *Nat. Struct. Mol. Biol. 20*, 1243−1249.
(28) Altschul, S. F., Madden, T. L., Schaffer, A. A., Zhang, J., Zhang, Z., Miller, W., and Lipman, D. J. (1997) Gapped blast and psi-blast: A new generation of protein database search programs. *Nucleic Acids Res. 25*, 3389−3402.
(29) Hammes-Schiffer, S., and Benkovic, S. J. (2006) Relating protein motion to catalysis. *Annu. Rev. Biochem. 75*, 519−541.
(30) Eisenmesser, E. Z., Millet, O., Labeikovsky, W., Korzhnev, D. M., Wolf-Watz, M., Bosco, D. A., Skalicky, J. J., Kay, L. E., and Kern, D. (2005) Intrinsic dynamics of an enzyme underlies catalysis. *Nature 438*, 117−121.
(31) Silva, R. G., Murkin, A. S., and Schramm, V. L. (2011) Femtosecond dynamics coupled to chemical barrier crossing in a Born-Oppenheimer enzyme. *Proc. Natl. Acad. Sci. U.S.A. 108*, 18661−18665.
(32) Siegel, J. B., Zanghellini, A., Lovick, H. M., Kiss, G., Lambert, A. R., St Clair, J. L., Gallaher, J. L., Hilvert, D., Gelb, M. H., Stoddard, B. L., Houk, K. N., Michael, F. E., and Baker, D. (2010) Computational design of an enzyme catalyst for a stereoselective bimolecular Diels-Alder reaction. *Science 329*, 309−313.
(33) Bhabha, G., Lee, J., Ekiert, D. C., Gam, J., Wilson, I. A., Dyson, H. J., Benkovic, S. J., and Wright, P. E. (2011) A dynamic knockout reveals that conformational fluctuations influence the chemical step of enzyme catalysis. *Science 332*, 234−238.
(34) Wang, Z., Abeysinghe, T., Finer-Moore, J. S., Stroud, R. M., and Kohen, A. (2012) A remote mutation affects the hydride transfer by disrupting concerted protein motions in thymidylate synthase. *J. Am. Chem. Soc. 134*, 17722−17730.

DOI: 10.1021/bi501487w
Biochemistry 2015, 54, 2520−2529